Available online at www.sciencedirect.com
SCIENCE DIRECT®
Journal of Nuclear Materials 350 (2006) 310–319
journal of nuclear materials
www.elsevier.com/locate/jnucmat

Evaluation of effect of hydrogen on toughness of Zircaloy-2 by instrumented drop weight impact testing

U.K. Viswanathan [a,*], R.N. Singh [b], C.B. Basak [c], S. Anantharaman [a], K.C. Sahoo [a]

[a] *Post Irradiation Examination Division, Bhabha Atomic Research Centre, Mumbai 400 085, India*
[b] *Materials Science Division, Bhabha Atomic Research Centre, Mumbai 400 085, India*
[c] *Radiometallurgy Division, Bhabha Atomic Research Centre, Mumbai 400 085, India*

Received 11 August 2005; accepted 28 January 2006

Abstract

Hydride-assisted degradation in fracture toughness of Zircaloy-2 was evaluated by carrying out instrumented drop-weight tests on curved Charpy specimens fabricated from virgin pressure tube. Samples were charged to 60 ppm and 225 ppm hydrogen. Ductile-to-brittle-transition behaviour was exhibited by as-received and hydrided samples. The onset of ductile-to-brittle-transition was at about 130 °C for hydrided samples, irrespective of their hydrogen content. Dynamic fracture toughness (K_{ID}) was estimated based on linear elastic fracture mechanics (LEFM) approach. For fractures occurring after general yielding, the fracture toughness was derived based on equivalent energy criterion. Results are supplemented with fractography. This simple procedure of impact testing appears to be promising for monitoring service-induced degradation in fracture toughness of pressure tubes.

PACS: 62.40.MK

1. Introduction

Zircaloy-2 tubes, which are now being replaced with Zr–2.5%Nb, are used as pressure tubes in Pressurized Heavy Water Reactors (PHWR) due to their low neutron absorption cross section, adequate mechanical properties at 300 °C and good resistance to aqueous corrosion. However, the main disadvantage of Zr-based alloys is their affinity to hydrogen that is produced from the corrosion reaction of the pressure tubes with water [1–6]. Hydrogen is also produced from the radiolytical decomposition of water in the ambience of intense radioactive field. Another source of hydrogen is the cathodic reaction between the stainless steel end fitting and the Zircaloy tube. Hydrogen enters the pressure tube either directly or by diffusion through the end fitting [5].

The solubility of hydrogen in zirconium at room temperature is very low and is less than 1 ppm by weight and the excess hydrogen precipitates as zirconium hydride, a brittle constituent [1–3].

* Corresponding author. Tel.: +91 22 2559 0659; fax: +91 22 2550 5151.
E-mail address: viswa@apsara.barc.ernet.in (U.K. Viswanathan).

0022-3115/$ - see front matter © 2006 Elsevier B.V. All rights reserved.
doi:10.1016/j.jnucmat.2006.01.016

Northwood and co-workers [4] have carried out an exhaustive review on the solubility of hydrogen in zirconium and its alloys, orientation and morphology of hydrides and their influence on mechanical properties. Because of the brittle nature and the characteristic thin platelet morphology, zirconium hydride is considered as a fracture initiator [7] and also aides in sub critical crack growth by the mechanism of delayed hydride cracking (DHC) [7,8].

Hydride-induced embrittlement of Zircaloy pressure tube is one of the serious life limiting issues in the operation of PHWRs. Embrittlement is manifested as reduction in the critical crack length leading to a premature fast failure of the tube [9]. A reliable prediction of critical crack length, based on the residual fracture toughness of the tube is highly desirable for the safe and economic operation of the reactor. Slit-burst tests on sections of pressure tubes are one of the established techniques for evaluating the critical crack length [10,11]. However, the slit-burst test requires large amount of material (minimum tube length of more than 300 mm of uniform properties for a single test) and also involves handling a large volume of irradiated material and associated complicated remote handling facility. Also, the number of data points that can be generated from each tube will be very small. Subsequently, test methods using 17 mm curved compact tension (CCT) specimens were developed by Chow and co-workers [12] for evaluating the fracture toughness of pressure tubes. *J*-integral resistance curve methods were used in both types of the above tests.

Conventional impact testing measures the total energy absorbed by a specimen during fracture. By instrumenting the striker the load–time (displacement) history of the specimen during the event of fracture can be evaluated. Objective of the present work is to evolve a simple method by using an instrumented drop weight impact testing machine to estimate the dynamic fracture toughness of pressure tubes from curved Charpy specimens of the type employed by Chow and co-workers [13]. As a first step of the feasibility study, the effect of different levels of hydrogen on the fracture toughness of Zircaloy-2 pressure tube is estimated by carrying out instrumented impact tests over a range of temperatures on curved Charpy type of specimens machined from a pressure tube. The values of maximum load, energy corresponding to maximum load and total absorbed energy in causing the fracture of the specimen were estimated from the load–time signal. Empirical estimation of dynamic fracture toughness was also attempted and the effect of hydrogen on fracture toughness evaluated. These results are supplemented with the examination of microstructure and fractographs.

2. Experimental procedure

2.1. Material and hydrogen charging

Zircaloy-2 tube used in this investigation is an off-cut from a pressure tube with 82.0 mm average internal diameter and 4.2 mm thickness. The fabrication route of the pressure tube, that imparted about 20% cold work in the finished product, included double vacuum arc melting, extrusion and two stages of cold pilgering with an intermediate annealing. The mean composition in wt% is 1.5 Sn, 0.12 Fe, 0.1 Cr, 0.05 Ni and 0.12 O. Spools of 50 mm length were cut from the tube and the inner and outer surfaces of the spools were polished using 1200 grit abrasive paper to obtain a fresh and oxide free surface. The polished spools were gaseously charged at 363 °C to the desired level with controlled amount of hydrogen in a modified Sievert's apparatus [14]. The spools after hydrogen charging were furnace cooled to room temperature. Hydrogen charging was carried out on two spools, to two nominal levels. The actual hydrogen content in the samples was estimated by inert gas fusion technique.

2.2. Curved Charpy specimens

Rings of 10 mm width were machined out from the unhydrided and hydrided spools. Curved specimens of $55 \times 10 \times 4.2$ mm for drop-weight tests were milled out from the rings. Four specimens were extracted from each ring. Dimensions of the curved Charpy specimens and their orientation with respect to the pressure tube are schematically shown in Fig. 1(a) and (b), respectively. The notch plane of the specimen was along the axial–radial plane of the tube so that the crack propagated along the axial direction of the tube, during fracture.

2.3. Metallography

Specimens from the undeformed end of the impact-tested samples were sectioned along axial–radial (longitudinal direction of the tube) and radial–circumferential (transverse direction of the

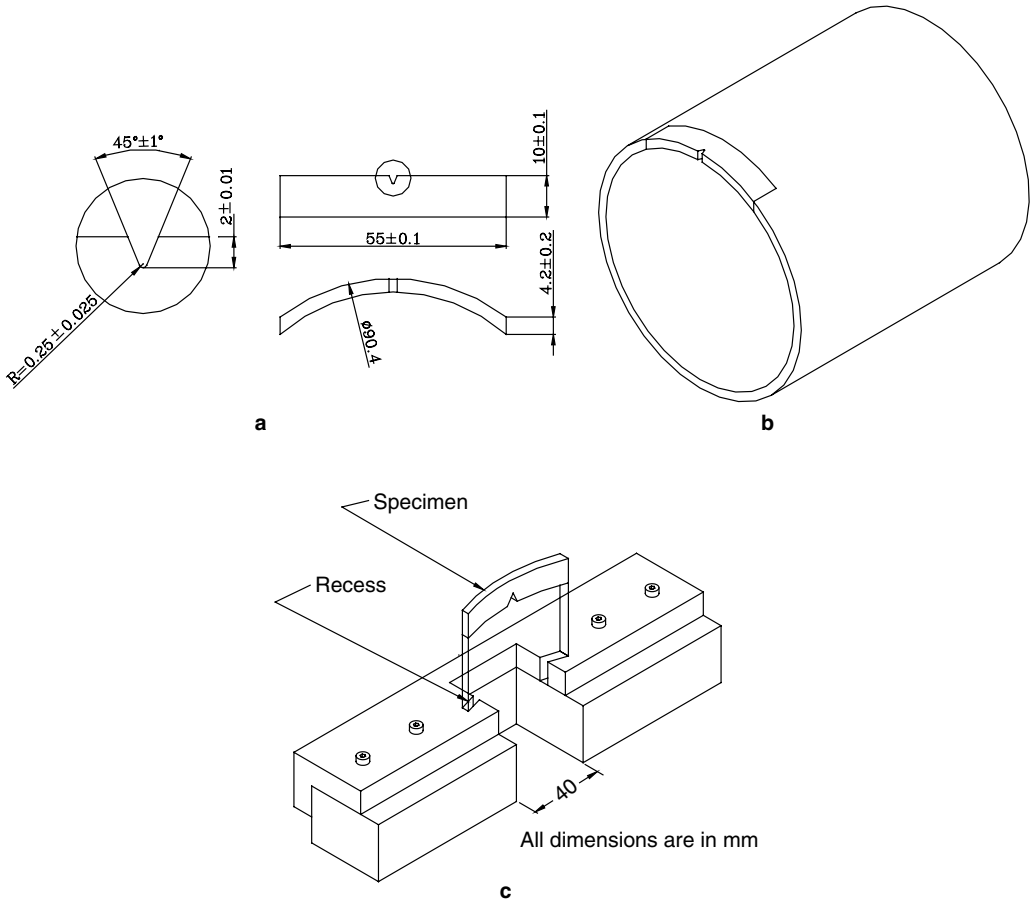

Fig. 1. Schematic diagrams of (a) curved Charpy specimen, (b) specimen location on the tube and (c) fixture for holding the specimen during test.

tube) planes of the pressure tube. Standard metallographic techniques were used to prepare the samples. Hydrides were revealed after swabbing for few seconds with an etchant of 8% HF in HNO_3.

2.4. Drop weight impact testing-methodology

An instrumented drop weight impact testing machine, with an environment chamber for thermal conditioning of the specimens, was used for testing. A specially designed anvil was fitted in place of standard Charpy anvil, located in the environment chamber. The anvil for holding the specimen and the exploded view of the specimen are schematically shown in Fig. 1(c). It is ensured that the specimen sits freely in the slot of the anvil at all temperatures of testing. Velocity of testing was 3.5 m/s (corresponding to a drop height of 0.625 m). To comply with the requirement to minimise velocity reduction during fracture, the available energy E_0 of the machine at this velocity of testing satisfied the conditions

$$E_0 \geqslant 3E_{\max\,\mathrm{load}} \quad \text{and} \quad E_0 > E_{\mathrm{T}},$$

where $E_{\max\,\mathrm{load}}$ is the energy absorbed by the specimen up to maximum load and E_{T} is the total energy required to completely fracture the specimen [15]. Specimens were heated for at least 45 min before testing to ensure thermal equilibrium at the test temperature. Tests were carried out from 32 °C (room temperature) to 288 °C, the operating temperature of the pressure tube.

The basic data generated during the test is the load–displacement plot. The area under the load–displacement plot provides the total energy to fracture. Depending on the deformation behaviour of the specimen, the total energy can be divided into crack initiation energy, which is the area under the load–displacement curve up to maximum load point and crack-propagation energy, which is the area

under the load–displacement curve from maximum load point up to complete fracture [16]. During the event of impact loading a crack is initiated at the root of the notch and extends laterally and reaches the edges of the specimen when maximum load is reached [17]. Several criteria are in vogue to precisely locate the crack initiation points on the dynamic load–displacement traces. Most of these criteria are based on experimental evidence obtained from dynamic tests carried out on pre-cracked Charpy specimens of standard geometry from pressure vessel steels [18,19]. Since there is no experimental procedure to determine the crack initiation point during an impact test, Server and co-workers assumed [16] that fracture initiates at maximum load point. Kobayashi [18] by conducting low-blow test has shown that crack initiation in a fatigue pre-cracked steel specimen occurs prior to the maximum load, at 80% of the maximum load. Ghoneim and Hammad [19] have reported that the fracture initiation occurs at an average load equal to $(P_{max} + P_{GY})/2$, where P_{max} is maximum load and P_{GY} is the load at general yielding of the specimen. Since no information on fracture behaviour of Zircaloy specimens of curved geometry and without pre-cracking is available, for inter-comparison purpose in this work P_{max} is taken as fracture initiation point and the energy up to the point corresponding to P_{max} is taken as crack initiation energy.

Dynamic fracture toughness (K_{ID}) was estimated by applying the conditions for linear elastic fracture mechanics (LEFM) and by applying the equation for three point bend specimens [20]:

$$K_{ID} = (6 \cdot P_M \cdot L \cdot \sqrt{a} \cdot Y)/(4B \cdot W^2), \quad (1)$$

where P_M is the applied load at fracture when fracture occurs before general yielding, L is the span width = 40 mm, a is the crack length = 2 mm, B is the thickness of the specimen = 4.2 mm, W is the width of the specimen = 10 mm and $Y = f(a/W) = 1.93 - 3.07(a/W) + 14.53(a/W)^2 - 25.11(a/W)^3 + 25.8(a/W)^4$.

For the fracture occurring after general yielding fracture toughness was derived based on equivalent energy approach [21]. It is assumed that if the specimen being used is thick enough to satisfy LEFM conditions, the fracture would have occurred before general yielding and the energy consumed would have been the crack initiation energy corresponding to the energy measured up to maximum load point. The fracture load P^* is estimated by extrapolating the linear slope of the elastic region of the load curve until the energy under the linear curve corresponds to the energy measured up to maximum load point. These P^* values are used in place of P_M in Eq. (1), for estimating dynamic fracture toughness [16].

2.5. Fractography

Fracture surfaces of broken Charpy samples were examined under scanning electron microscope (SEM).

3. Results

3.1. Hydrogen content and hydride distribution

Hydrogen content (by weight) in the as received material was 10 ppm. Other 2 spools contained 60 ppm and 225 ppm of hydrogen. Hydrogen charging was fairly uniform in the spools. Fig. 2(a)–(c) shows the hydride distribution along the axial–radial plane of the spools with different levels of hydrogen. Dark lines in these micrographs are the traces of hydride platelets, which are preferentially aligned along the axial direction of the tube. With increase in hydrogen content the length of the hydride platelets increased and their number density moderately increased. The corresponding hydride distribution along the radial–circumferential plane of the spools is shown in Fig. 3(a)–(c). In general, the traces of hydride platelets on the axial–radial plane were straighter and longer than the traces observed on the radial–circumferential plane.

3.2. Drop-weight test

Typical load–deformation (displacement) plots generated during drop-weight tests at different temperatures on curved specimens of Zircaloy-2 with different hydrogen contents are shown in Fig. 4(a)–(c). Improved ductility with increasing test temperatures can clearly be noticed for all the specimens. It is evident from the plot shown in Fig. 4(a) that at room temperature (32 °C) as-received material fractured in a fully ductile manner, showing general yielding followed by a maximum load and a gradual load drop till complete separation. The load–displacement plot for the hydrided specimens showed a significant reduction in displacement to failure. Samples with 60 ppm and 225 ppm hydrogen exhibited typical brittle fracture at room temperature, with the load dropping abruptly from

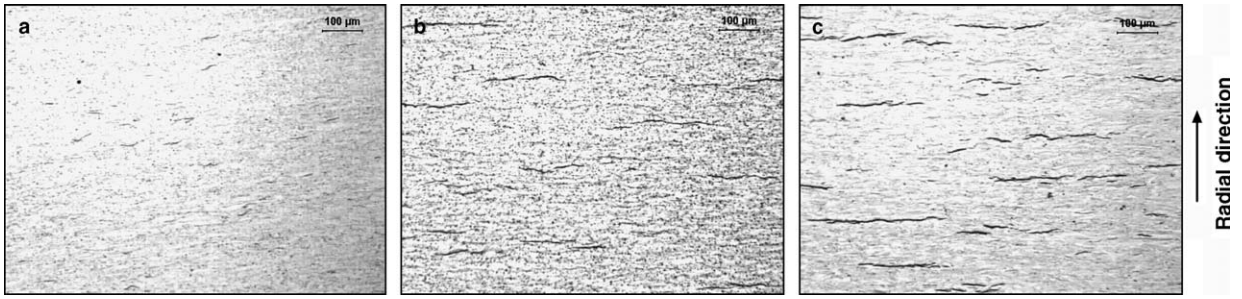

Fig. 2. Hydride distribution in axial–radial plane Zircaloy-2 in (a) as-received, (b) with 60 ppm hydrogen and (c) with 225 ppm hydrogen.

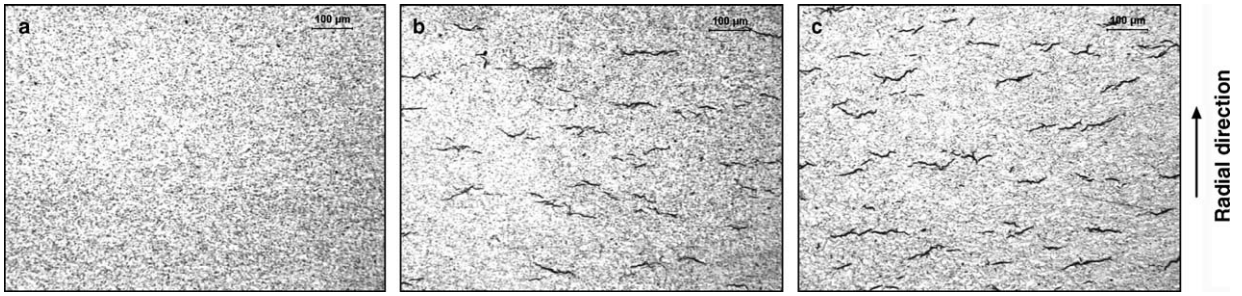

Fig. 3. Hydride distribution in radial–circumferential plane Zircaloy-2 in (a) as-received, (b) with 60 ppm hydrogen and (c) with 225 ppm hydrogen.

the peak load to zero load, as shown in Fig. 4(b) and (c), the drop being more abrupt for sample with 225 ppm hydrogen. At 200 °C, sample with 60 ppm hydrogen fractured in a semi-brittle manner, showing some yielding before the load dropping to zero, while the sample with 225 ppm hydrogen failed almost abruptly at the peak load.

Energy absorbed till fracture by the material in as-received and in hydrided conditions, plotted against test temperature is shown in Fig. 5. For as-received samples, the transition from brittle to ductile mode of failure is gradual compared to hydrided material. The effect of hydrogen on embrittling Zircaloy-2 by way of shift in the ductile–brittle transition temperature to higher temperature and reduction in upper shelf energy is evident from the respective positions of the curves along the temperature axis. Sharp transitional behaviour is exhibited by samples with 60 ppm and 225 ppm hydrogen. At 288 °C energy absorbed by the material containing 60 ppm hydrogen almost equaled the energy of unhydrided Zircaloy. At all temperatures of testing, samples with 225 ppm hydrogen showed lower toughness than samples with 60 ppm hydrogen. However, the onset of brittle-to-ductile transitional behaviour was noticed at about 130 °C for hydrided materials, irrespective of their hydrogen content.

The crack initiation energy and the crack-propagation energy derived from the data of Fig. 4(a)–(c) are plotted against test temperature and are shown in Figs. 6 and 7, respectively. Though the transitional behaviour is exhibited by both components of energy, propagation energy transition behaviour is found to be sharper for hydrided material and is similar to total-energy-based transition behaviour.

Fig. 8 shows the dynamic fracture toughness, K_{ID}, estimated up to the onset of brittle to ductile transition from the load–deformation traces for the hydrided and unhydrided samples. Room temperature fracture toughness was 63 $MPa\sqrt{m}$ for unhydrided material, 36 $MPa\sqrt{m}$ for Zircaloy with 60 ppm and 34 $MPa\sqrt{m}$ for Zircaloy with 225 ppm of hydrogen. The K_{ID} values were observed to increase mildly with increase in test temperature, though the increase in K_{ID} values for hydrided samples were insignificant.

3.3. Fractography

Fractographs of the broken Charpy specimens tested at room temperature, 200 °C, 225 °C and

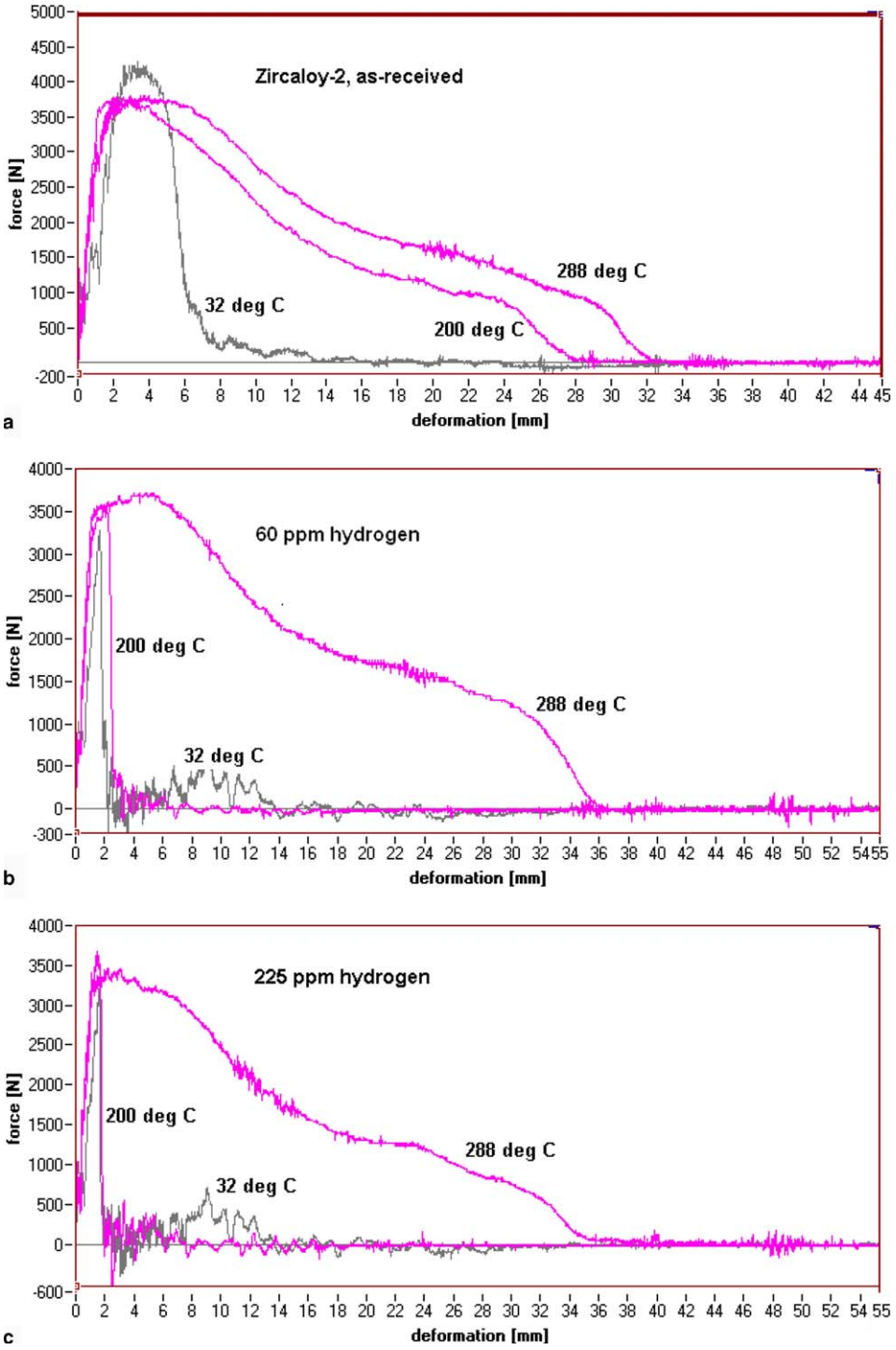

Fig. 4. Load–deformation plots obtained during drop-weight test at different temperatures on Zircaloy-2 samples in (a) as-received, (b) with 60 ppm and (c) 225 ppm hydrogen.

288 °C are shown in Figs. 9–12, respectively. The crack growth direction is from right to left in the fractographs. The fracture surface of unhydrided specimens tested at room temperature showed a ductile failure caused by micro-void coalescence (Fig. 9(a)). Hydrided specimens showed a mixed

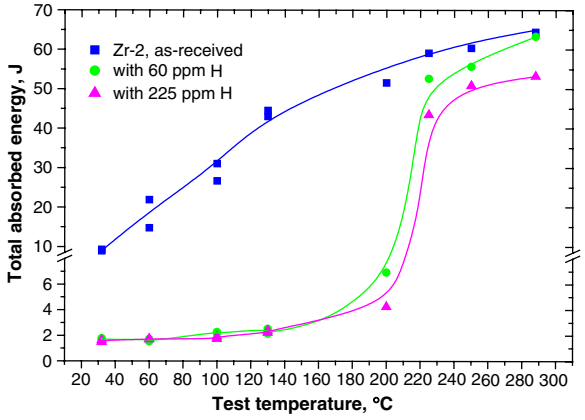

Fig. 5. Total absorbed energy as function of test temperature.

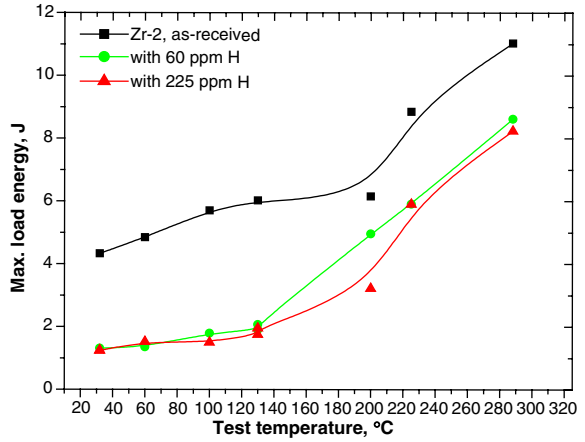

Fig. 6. Crack initiation energy as function of test temperature.

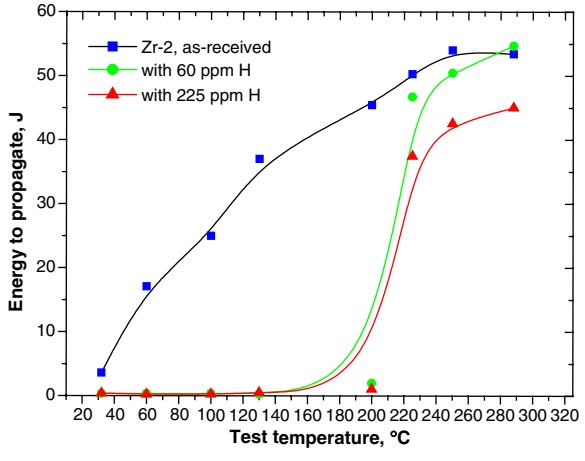

Fig. 7. Crack-propagation energy as function of test temperature.

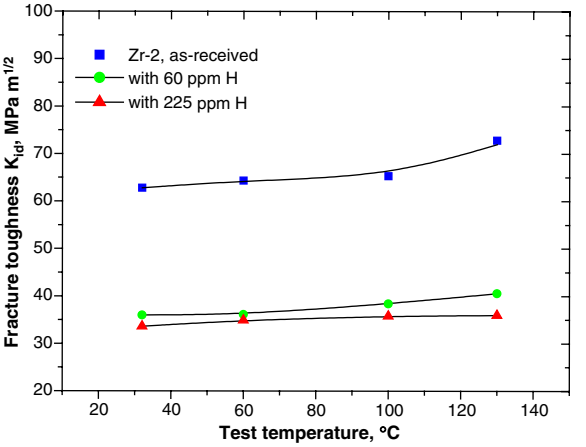

Fig. 8. Dynamic fracture toughness as function of test temperature.

fracture mode of ductile tearing of the matrix, interspaced with near-parallel and linear cracks (Fig. 9(b) and (c)). The presence of a number of linear cracks noticed on the fracture surfaces of the hydrided specimens is suggestive of the fracture being assisted by the hydride platelets. Relatively large number of interconnected cracks was noticed on the fracture surface of specimens with 225 ppm hydrogen than that with 60 ppm hydrogen. At 200 °C, the mode of failure was predominantly by micro-void coalescence, interspaced with hydride-assisted cracks (Fig. 10). With a small increase in the test temperature from 200 °C to 225 °C, a marked change in the fracture behaviour could be noticed in hydrided and unhydrided samples. Samples tested at 225 °C and 288 °C exhibited totally fibrous fracture surfaces, irrespective of the hydrogen content, as shown in Figs. 11(a)–(c) and 12(a)–(c). The fracture of the samples appeared to be caused by the ductile tearing of the zirconium matrix. The type of cracks noticed in hydrided samples tested at room temperature and 200 °C were not observed in specimens tested at 225 °C and 288 °C.

4. Discussion

The hydride orientation with respect to any residual or applied stresses has a large influence on the impact strength and fracture toughness of zirconium alloys [4]. Two types of hydride orientations, namely the circumferential and radial, have been found in zirconium-alloy pressure tubes [4]. During reactor service, radial hydrides can offer poor resistance to fracture under the prevailing hoop stress. A

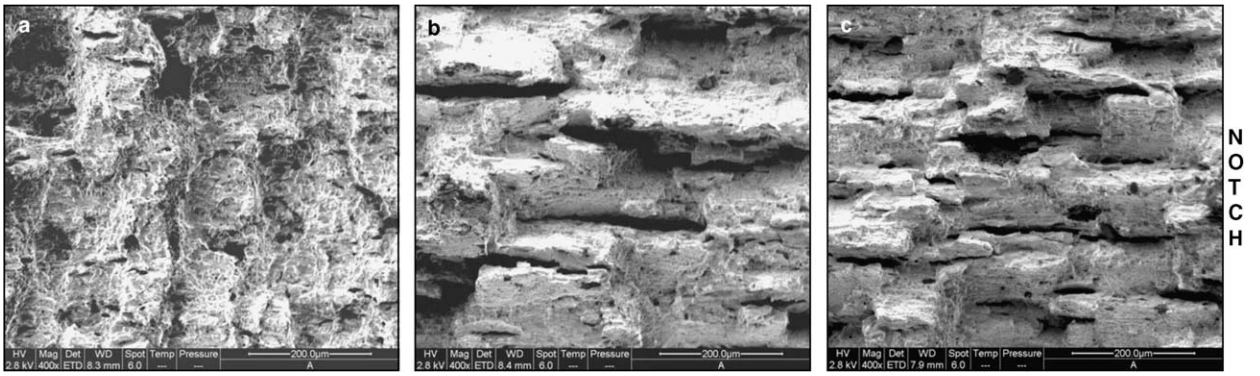

Fig. 9. Fractograph of Charpy specimens tested at room temperature from Zircaloy-2: (a) unhydrided, (b) with 60 ppm and (c) with 225 ppm hydrogen.

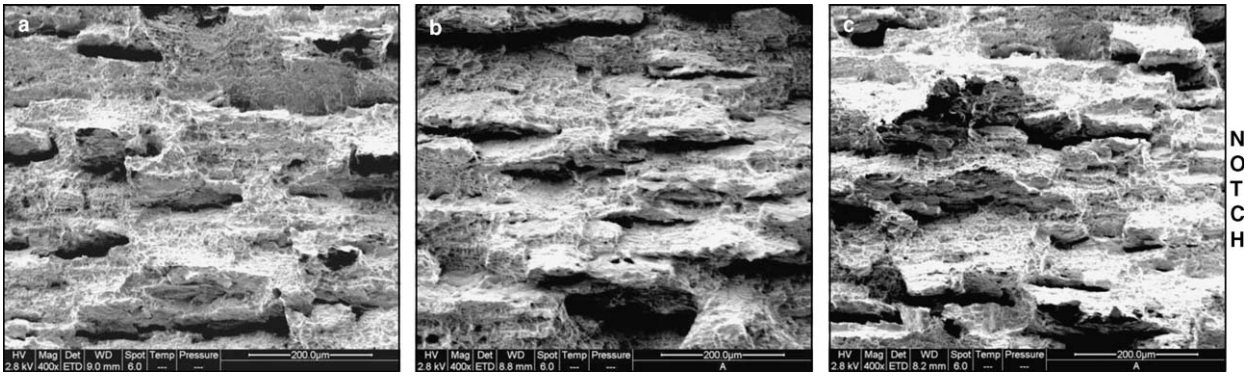

Fig. 10. Fractograph of Charpy specimens tested at 200 °C from Zircaloy-2: (a) unhydrided, (b) with 60 ppm and (c) with 225 ppm hydrogen.

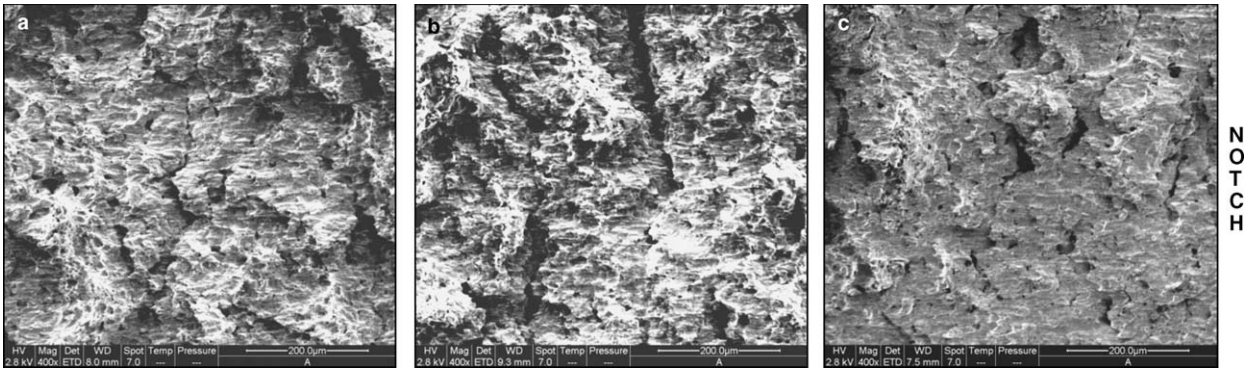

Fig. 11. Fractograph of Charpy specimens tested at 225 °C from Zircaloy-2: (a) unhydrided, (b) with 60 ppm and (c) with 225 ppm hydrogen.

pressure tube with hydrides oriented predominantly in radial direction can undergo a fast fracture under such a condition. However, the extrusion and cold pilgerings techniques used in the fabrication of the tubes have produced tubes with a texture that enabled hydride platelets formation predominantly along the circumferential direction, as observed in this study (Figs. 2 and 3).

The decrease in impact toughness in hydrided material at temperatures below the ductile-to-brittle

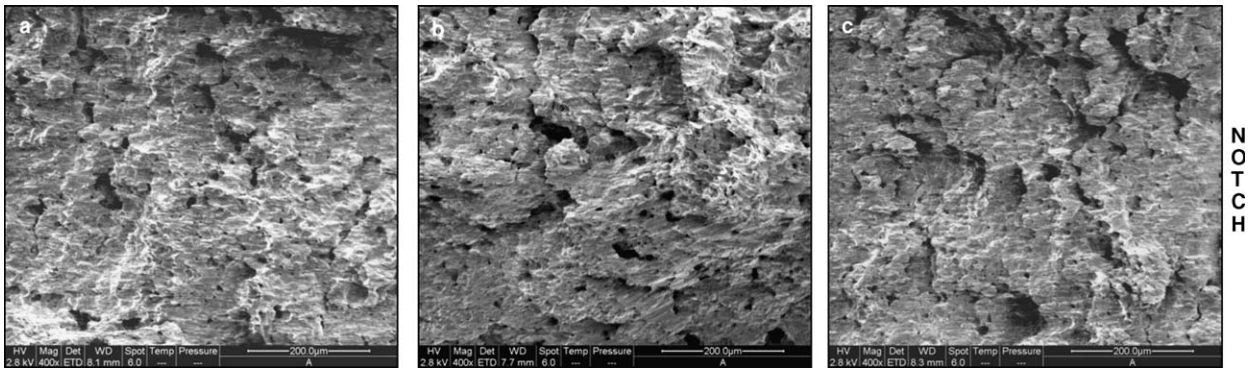

Fig. 12. Fractograph of Charpy specimens tested at 288 °C from Zircaloy-2: (a) unhydrided, (b) with 60 ppm and (c) with 225 ppm hydrogen.

transition region is associated with the splitting of hydride platelets along the direction of crack propagation, as shown in the fracture surfaces of impact specimens (Fig. 9(b) and (c)). The splitting, which occurred perpendicular to the plane of crack propagation has left fissures with vertically slanted lips on the fracture surfaces. It is interesting to note that the length and width of these fissures matched well with those of the hydride platelets in the axial–radial plane (Fig. 2(b) and (c)). The energy transition curves based on total absorbed energy (Fig. 5) and crack-propagation energy (Fig. 7) for hydrided materials showed sharp transition compared to unhydrided Zircaloy. For hydrided zirconium alloys, the transition from brittle to ductile mode of failure, with increase in test temperature is not associated with the failure mode changing from cleavage to shear, as generally observed in ferritic steels [22]. When the test temperature is increased, zirconium takes more hydrogen into solution till the corresponding terminal solubility is attained. In the case of as-received material, the initial hydrogen content of 10 ppm dissolves in the matrix at about 190 °C [23] and therefore, the energy to fracture, above this temperature, is decided by the toughness of Zircaloy matrix. It is observed that the total-energy-transition curve for unhydrided Zircaloy reached a saturation level above 190 °C.

Zircaloy with 60 ppm hydrogen has shown severe embrittlement, which is manifested as an upward shift in the ductile-to-brittle transition temperature. Sharp recovery in toughness is noticed above 200 °C. Based on investigation carried out on irradiated Zircaloy-2 pressure tubes, Huang [1] has proposed that hydride precipitates provide sites for easy crack nucleation and delamination. Hydride platelets influence crack propagation either by decreasing the work hardening or by increasing the cavity growth rate, thereby causing a reduction in ductility. Due to increased solubility of hydrogen with increasing temperature, part of the hydride platelets start dissolving, bringing about a decrease in platelet size or/and its number density. An increase in inter-platelet distance makes the crack propagation difficult. The ductility of the Zircaloy matrix also increases with increasing temperature. The recovery in toughness above 200 °C can be attributed mainly to the improved ductility of zirconium matrix, as zirconium hydride does not significantly become ductile above 150 °C [4]. Solubility of hydrogen in zirconium is 65 ppm at 300 °C [23]. At 288 °C the upper shelf energy of sample with 60 ppm hydrogen equaled that of unhydrided material, suggesting that hydrogen has completely gone into solution at this temperature of testing. The fracture surfaces of the samples tested at 225 °C and 288 °C (Figs. 11(b) and 12(b), respectively) did not show the presence of any fissures associated with the splitting of hydride platelets.

Above 60 ppm the effect of hydrogen on embrittlement is found to be marginal. With 225 ppm hydrogen, the material showed only an additional shift of about 10 °C over the entire transition portion of the curve. However, at 288 °C Zircaloy with 225 ppm hydrogen possessed lower upper shelf energy than the material with 60 ppm hydrogen, as can be noticed from Fig. 5. As the hydrogen content is more than the solubility limit at this temperature of testing, some hydride platelets are expected to be present in the microstructure. The observed decrease in the upper shelf energy could be due to the presence of hydride platelets in the material.

However, the fracture surface of the samples tested at 225 °C and 288 °C did not contain any fissures caused by the splitting of hydride platelets (Figs. 11(c) and 12(c), respectively).

The Charpy V-notch specimens used in this work do not satisfy the size requirements for valid plane strain fracture toughness for the material. Irrespective of the numerical accuracy, the measured fracture toughness values can be used for inter-comparison of samples tested at different temperatures and with different hydrogen contents. The room temperature fracture toughness of 63 MPa$\sqrt{m}$ obtained for the unhydrided Zircaloy-2 in this work compares well with the value of 87 MPa$\sqrt{m}$ estimated from ring tension test conducted on samples from another pressure tube, produced through the same fabrication route [24]. The lower fracture toughness value obtained in this work could be due to the dynamic straining employed in this work.

5. Conclusions

The following conclusions could be drawn from this work:

1. Instrumented drop-weight test on curved Charpy specimens machined from pressure tube can be used to monitor service-induced degradation in fracture toughness of pressure tubes.
2. Ductile-to-brittle energy-transition behaviour was exhibited by as-received and hydrided Zircaloy-2. Hydrided material showed a sharp transitional behaviour. At 288 °C energy absorbed by the material containing 60 ppm hydrogen almost equaled the energy absorbed by unhydrided Zircaloy for fracture.
3. At all temperatures of testing, samples with 225 ppm hydrogen showed lower toughness than samples with 60 ppm hydrogen. However, the onset of brittle-to-ductile transitional behaviour was noticed at about 130 °C for hydrided materials, irrespective of their hydrogen content.
4. The fracture surfaces of the samples tested at room temperature and at 200 °C showed features suggestive of hydride-assisted failure. However, the samples tested at the upper shelf energy region did not show any evidence of hydride-assisted failure.
5. Dynamic fracture toughness at room temperature estimated by using equivalent energy approach was 63 MPa$\sqrt{m}$ for unhydrided Zircaloy-2, 36 MPa$\sqrt{m}$ for Zircaloy with 60 ppm and 34 MPa$\sqrt{m}$ for Zircaloy with 225 ppm of hydrogen.

References

[1] F.H. Huang, J. Nucl. Mater. 207 (1993) 103.
[2] C.E. Coleman, D. Hardie, J. Less Common Met. 11 (1966) 168.
[3] C.E. Ells, J. Nucl. Mater. 28 (1968) 129.
[4] D.O. Northwood, U. Kosasih, Int. Metals Rev. 28 (2) (1983) 92.
[5] L.A. Simpson, C.E. Coleman, Nucl. Eng. Des. 137 (1992) 437.
[6] R.N. Singh, S. Mukherjee, A. Gupta, S. Banerjee, J. Alloys Compd. 389 (2005) 102.
[7] G. Bertolino, G. Meyer, J. Perez Ipina, J. Nucl. Mater. 322 (2003) 57.
[8] R.N. Singh, N. Kumar, R. Kishore, S. Roychowdhury, T.K. Sinha, B.P. Kashyap, J. Nucl. Mater. 304 (2002) 189.
[9] A. Cowan, W.J. Langford, J. Nucl. Mater. 30 (1969) 271.
[10] A. Cowan, K.J. Cowburn, J. Inst. Metals 95 (1967) 302.
[11] W.J. Langford, L.E.J. Mooder, Int. J. Pressure Vessels Piping 6 (1978) 275.
[12] C.K. Chow, L.A. Simpson, in: D.T. Read, R.P. Reed (Eds.), Fracture Mechanics: Eighteenth Symposium, ASTM STP 945, ASTM, Philadelphia, 1988, pp. 419–439.
[13] C.K. Chow, C.E. Coleman, R.R. Hosbons, P.H. Davies, M. Griffiths, R. Choubey, in: C.M. Eucken, A.M. Garde (Eds.), Zirconium in the Nuclear Industries: Ninth International Symposium, STP 1132, ASTM, Philadelphia, 1991, pp. 246–275.
[14] R.N. Singh, PhD Thesis, Indian Institute of Technology, Mumbai, India, 2002.
[15] D.R. Ireland, Suggested Method of Test for Impact Test of Precracked Charpy Specimens of Metallic Materials, Tech. Rep. T.R.79-58, Effects Technology, Inc., Santa Barbara, CA93105, February 1979.
[16] W.L. Server, D.R. Ireland, R.A. Wullaert, Strength and Toughness Evaluations from an Instrumented Impact Test, Tech. Rep. T.R.74-29R, Effects Technology, Inc., Santa Barbara, CA93111, November 1974.
[17] A. Fabry, E. van Walle, J. van de Velde, R. Chaouadi, J.L. Puzzolante, Th. van Ransbeeck, A. Verstrepen, in: E. van Walle (Ed.), Evaluating Material Properties by Dynamic Testing, ESIS20, Mechanical Engineering, London, 1996, pp. 59–78.
[18] T. Kobayashi, Eng. Fract. Mech. 19 (1) (1984) 49.
[19] M.M. Ghoneim, F.H. Hammad, J. Nucl. Mater. 186 (1992) 196.
[20] T.J. Koppenaal, in: D.R. Ireland (Ed.), Instrumented Impact Testing: Symposium at the seventy sixth annual meeting, ASTM STP 563, ASTM, Philadelphia, 1974, pp. 92–117.
[21] F.J. Witt, Eng. Fract. Mech. 14 (1981) 171.
[22] M. Farrow, B. Watkins, J. Nucl. Mater. 15 (3) (1965) 208.
[23] J.J. Kearns, J. Nucl. Mater. 22 (1967) 292.
[24] S. Chatterjee, K.S. Balakrishnan, Priti Kotak Shah, Report BARC/2004/E/007, Bhabha Atomic Research Centre, Mumbai, India, 2004.